REPORT DOCUMENTATION PAGE

Form Approved
OMB No. 0704-0188

1. AGENCY USE ONLY *(Leave blank)*	2. REPORT DATE	3. REPORT TYPE AND DATES COVERED
	15 January 2000	Final Report 17 May 99 - 30 Sept 99

4. TITLE AND SUBTITLE
Electromagnetic Interaction, Thermal and Mass Transfer Modeling of the Photothermal Modulation of Mie Scattering Spectroscopy of Aerosols

5. FUNDING NUMBERS
Grant No.
N00173-99-G009
PR No. 56-1906-99

6. AUTHORS
John P. Barton

7. PERFORMING ORGANIZATION NAME(S) AND ADDRESS(ES)
University of Nebraska-Lincoln
Sponsored Programs Office
306 Administration Building
Lincoln, NE 68588-0430

8. PERFORMING ORGANIZATION REPORT NUMBER
LWF/11-188-13101

9. SPONSORING/MONITORING AGENCY NAME(S) AND ADDRESS(ES)
Department of the Navy
Naval Research Laboratory
4555 Overlook Avenue, SW
Washington, DC 20375-5326
Program Officer:
Dr. Anthony J. Campillo

10. SPONSORING/MONITORING AGENCY REPORT NUMBER

11. SUPPLEMENTARY NOTES

12a. DISTRIBUTION/AVAILABILITY STATEMENT
Approved for Public Release

12b. DISTRIBUTION CODE

13. ABSTRACT *(Maximum 200 words)*

Theoretical procedures were developed, computer programs were written, and demonstration calculations were performed investigating the modeling and predicted performance of the photothermal modulation of Mie scattering (PMMS) spectroscopy method for aerosol diagnostics.

14. SUBJECT TERMS
Mie scattering, aerosol diagnostics, particle sizing, laser/droplet interaction

15. NUMBER OF PAGES
24

16. PRICE CODE

17. SECURITY CLASSIFICATION OF REPORT	18. SECURITY CLASSIFICATION OF THIS PAGE	19. SECURITY CLASSIFICATION OF ABSTRACT	20. LIMITATION OF ABSTRACT

ELECTROMAGNETIC INTERACTION, THERMAL AND MASS TRANSFER MODELING OF THE PHOTOTHERMAL MODULATION OF MIE SCATTERING (PMMS) SPECTROSCOPY OF AEROSOLS

FINAL REPORT

JANUARY 15, 2000

PRINCIPAL INVESTIGATOR
Dr. John P. Barton, Associate Professor
Department of Mechanical Engineering
College of Engineering & Technology
University of Nebraska-Lincoln
Lincoln, Nebraska 68588-0656
Ph# (402) 472-5081
Fax# (402) 472-1465
Email jbarton@unlserve.unl.edu

SPONSORING AGENCY
Department of the Navy
Naval Research Laboratory
4555 Overlook Avenue, SW
Washington, DC 20375-5326
Program Officer: Dr. Anthony J. Campillo
Grant No. N00173-99-1-G009
PR No. 56-1906-99

"Electromagnetic Interaction, Thermal and Mass Transfer Modeling of the Photothermal Modulation of Mie Scattering (PMMS) Spectroscopy of Aerosols"

John P. Barton
University of Nebraska-Lincoln
January 15, 2000

I. Introduction

The procedure of photothermal modulation of Mie scattering (PMMS) spectroscopy is a promising technique that can potentially provide the sensitive *in situ* measurement of important aerosol characterization parameters such as particle size distribution, index-of-refraction, and composition. In the PMMS procedure, the intensity of an infrared laser beam (e.g., a CO_2 laser) is modulated in time (i.e., chopped) and passed through the aerosol cloud. The diameters of the droplets in the aerosol cloud subsequently also modulate in time due the associated time-varying heating, evaporation, and recondensation. A second laser beam, in this case a visible light laser beam (e.g., a He-Ne laser), is passed through the aerosol cloud and the effect of the time-variation of the droplet diameters due to the modulated infrared laser heating is observed by monitoring the time-variation of the elastically scattered light. The actual time-variation of droplet diameter will be a function of the droplet nominal diameter, the droplet index of refraction (including absorption), the modulation frequency, the laser intensity, and the droplet liquid and surrounding medium thermal and mass transfer properties. The work reported here provides theoretical modeling of the PMMS procedure that will a.) assist in developing the relationship between the measured modulated elastically scattered light and the aerosol cloud properties, b.) assist in optimizing PMMS design parameters, and c.) assist in verifying physical understanding through the comparison of theoretical predictions with corresponding controlled experimental measurements.

Section II. describes the theoretical thermal and mass transfer modeling for a single droplet heated by an intensity modulated laser beam. In Sec. III., the elastic light scattering from a polydispersed aerosol cloud with modulated heating is considered. A set of demonstration calculations are presented and examined in Sec. IV. and a discussion of possible future work is given in Sec. V. Section VI. contains a list of references.

II. Single Particle Modeling

The following basic assumptions are made.

1.) The droplet is spherical and consists of a solution of a nonvolatile solute (e.g., NaCl) in a volatile solvent (e.g., water).
2.) The surrounding medium is moist air with time-invariant temperature and relative humidity.
3.) Plane wave illumination on the droplet by the infrared (heating) and visible (scattering) laser beams is assumed.
4.) The droplet has a single uniform temperature.
5.) The heat and mass transfer processes at the surface of the droplet are described using a quasi-steady, boundary layer model.
6.) A form of Raoult's law is used to determine the vapor pressure at the droplet's surface.

The notation is as follows.

c_d = specific heat per mass of droplet solution
$D = 2\, r_{do}$, droplet initial diameter
D_L = log-normal distribution mean diameter
D = mass diffusion coefficient for vapor in air
$\vec{E}$ = electric field vector of elastic scattered light
h_{fg} = enthalpy of evaporation of solvent
$\vec{H}$ = magnetic field vector of elastic scattered light
I_{abs} = time dependent intensity of the infrared (heating) laser beam
I_{sca} = intensity of the visible (elastic scattering) laser beam
k = thermal conductivity of moist air
$m_d = (m_w + m_s)$ = droplet mass
$m_s = m_{so}$ = mass of solute in droplet (time-invariant)
m_w = mass of solvent in droplet
m_{wo} = initial mass of solvent in droplet
M_w = molecular weight of solvent
M_s = molecular weight of solute
$\dot{m}_v''$ = mass flux of vapor at the droplet surface (positive outward)
m_{liq} = initial mass of aerosol liquid in elastic scattering probe volume
N = number of droplets in elastic scattering probe volume
$\bar{n}_{abs}$ = complex index of refraction of droplet at the infrared wavelength
$\bar{n}_{sca}$ = complex index of refraction of droplet at the visible wavelength
$p(D)$ = probability density function of initial aerosol size distribution
p_g = saturation pressure of solvent
$p_{v,d}$ = vapor pressure at droplet surface
$p_{v,\infty}$ = vapor pressure at ambient condition
p_∞ = ambient pressure
Q_{abs} = droplet absorption efficiency at infrared (heating) laser wavelength
$\dot{q}''$ = heat flux due to conduction at the droplet surface (positive outward)
r_d = droplet radius
r_{do} = initial droplet radius

R_v = gas constant for vapor
T_d = droplet temperature
T_{do} = initial droplet temperature
T_f = film temperature of the boundary layer above the droplet surface = $(T_d + T_\infty) / 2$
T_∞ = temperature of the ambient air
$\bar{V}_{d0}$ = average droplet volume of initial aerosol distribution
λ_{abs} = wavelength of infrared (heating) laser beam
λ_{sca} = wavelength of visible (scattering) laser beam
θ_{dir} = polar angle direction of observed elastic scattered light
ρ_d = mass density of droplet solution
$\rho_{v,d}$ = mass density of vapor at the droplet surface
$\rho_{v,\infty}$ = mass density of vapor in the ambient air
σ_{DL} = log-normal distribution standard deviation parameter
ϕ_∞ = relative humidity of the vapor in the ambient air
ϕ_{dir} = azimuthal angle direction of observed elastic scattered light

An application of conservation of energy for the droplet provides the following equation for the time rate of change of the droplet temperature,

$$\frac{dT_d}{dt} = \frac{1}{(m_d\, c_d)}[\, I_{abs}(\pi r_d^2) Q_{abs} - \dot{m}_v''(4\pi r_d^2) h_{fg} - \dot{q}''(4\pi r_d^2)\,] \tag{1}$$

where the three terms on the right-hand-side represent, respectively, the rate of laser heating, the rate of evaporative cooling, and the rate of conductive cooling. In addition, the time rate of change of the mass of the solvent of droplet is the negative of the rate of solvent evaporation,

$$\frac{dm_w}{dt} = -\,\dot{m}_v''(4\pi r_d^2) \tag{2}$$

The heat flux and mass flux at the droplet surface are evaluated using a quasi-steady boundary layer assumption so that

$$\dot{m}_v'' = (\frac{1}{r_d}) D(\rho_{v,d} - \rho_{v,\infty}) \tag{3}$$

and

$$\dot{q}'' = (\frac{1}{r_d}) k(T_d - T_\infty) \tag{4}$$

where in Eq. (3),

$$\rho_{v,\infty} = \frac{p_{v,\infty}}{R_v T_\infty} \tag{5}$$

and

$$\rho_{v,d} = \frac{p_{v,d}}{R_v T_d} \tag{6}$$

where

$$p_{v,\infty} = \phi_\infty p_g(T_\infty) \tag{7}$$

and

$$p_{v,d} = \frac{1}{[1 + 2(M_w/M_s)(m_{s0}/m_w)]} p_g(T_d) \tag{8}$$

Equation (8) is a representation of Raoult's law, where the assumption is made that the vapor pressure of the solvent at the droplet surface is equal to the saturation pressure of the vapor at the droplet temperature times the mole fraction of the solvent within the droplet. The factor of 2 in the denominator of Eq. (8) occurs with the assumption that the solute is ionic, and thus each molecule of solute effectively divides into 2 separate ion molecules.

Before the laser heating is initiated, it is assumed that the droplet is in equilibrium (both thermally and with regard to composition) with the surroundings. The initial mass ratio of solute to solvent within the droplet is thus determined by equating Eqs. (7) and (8) with the initial condition that $T_d = T_\infty$,

$$(m_{so}/m_{wo}) = \frac{(1-\phi)}{2\phi}(M_s/M_w) \tag{9}$$

For a droplet of initial radius, r_{do}, the initial mass of solvent and solute then can be found in terms of this ratio,

$$m_{w0} = \rho_{d0}(4\pi/3) r_{d0}^3 / [1 + (m_{s0}/m_{w0})] \tag{10}$$

and

$$m_{s0} = m_{w0}(m_{s0}/m_{w0}) \tag{11}$$

Finally, since the total mass of the droplet is the sum of the mass of the solute (which is constant) and the mass of the solvent (which varies in time), if the mass of the solvent in known, then the radius of the droplet can be determined from

$$r_d = \left[\frac{(m_w + m_{s0})}{(4\pi/3)\rho_d}\right]^{1/3} \tag{12}$$

Beginning with a droplet of known radius, Eqs. (9) - (11) are used to find the initial mass of solvent and mass of solute within the droplet. Once the laser heating starts, the time variations of droplet temperature, size, and composition are determined by solving Eqs. (1) and (2) [along

with the associated Eqs. (3) - (8) and (12)], using a finite difference predictor-corrected method to "march" along in time. The following property relationships are also required:
$c_d = func\,(T_d)$, $h_{fg} = func\,(T_d)$, $D = func\,(T_f, p_\infty)$, $k = func\,(T_f)$,
$\rho_d = func\,(T_d, (m_s/m_w))$, $Q_{abs} = func\,(r_d, \lambda_{abs}, \bar{n}_{abs})$, and $\bar{n}_{abs} = func(\lambda_{abs}, (m_s/m_w))$ where $T_f = (T_d + T_\infty)/2$ is the boundary layer film temperature.

III. Elastic Scattering from a Polydispersed Aerosol

The nondimensionalized far-field elastic light scattering intensity in the $(\theta_{dir}, \phi_{dir})$ direction (relative to the propagation direction of the incident elastic scattering laser beam) for a single droplet can be determined from Lorenz-Mie theory and is given by

$$\tilde{S}_r = \lim_{r/r_d \to \infty} (r/r_d)^2 (\frac{c}{8\pi}) Re(\vec{E} \times \vec{H}^*)_r / I_{sca} = func\,(\theta_{dir}, \phi_{dir}, r_d, \lambda_{sca}, \bar{n}_{sca}) \tag{13}$$

where $\bar{n}_{sca} = func\,(\lambda_{sca}, (m_s/m_w))$. If p(D) is the initial droplet size distribution for the aerosol, then

$$\overline{V}_{d0} = (\frac{\pi}{6}) \int_{-\infty}^{\infty} D^3 p(D) dD \tag{14}$$

provides the average droplet volume in the initial distribution and the number of droplets in the probe volume is then given by

$$N = \frac{m_{liq}}{\rho_{d0} \overline{V}_{d0}} \tag{15}$$

where m_{liq} is the initial amount of aerosol liquid in the elastic scattering probe volume. An expression for the total elastic scattering for the aerosol can then be determined by integrating over the individual droplet scattering as follows

$$\tilde{S}_r)_{tot} = \frac{r^2 S_r)_{tot}}{m_{liq} I_{sca}} = \frac{1}{\rho_{d0} \overline{V}_{d0}} \int_0^{\infty} r_d^2 \tilde{S}_r\, p(D) dD \tag{16}$$

While any aerosol size distribution may be assumed, for the calculations presented in Sec. IV., a log-normal size distribution was used where

$$p(D) = \frac{1}{\sqrt{2\pi}\, D\, \sigma_{DL}} exp\Big\{ - \frac{[ln(D/\bar{D}_L)]^2}{2\sigma_{DL}^2} \Big\} \tag{17}$$

$$ln(\bar{D}_L/D_{ref}) = \overline{ln(D/D_{ref})} \tag{18}$$

and

$$\sigma_{DL} = \{ \overline{[ln(D/\bar{D}_L)]^2} \}^{1/2} \tag{19}$$

where the overbar indicates a size distribution averaged quantity. As an example, Fig. 1 shows a log-normal distribution for an aerosol with a log-normal mean diameter ($\bar{D}_L$) of 2.0 microns and a log-normal distribution standard deviation parameter (σ_{DL}) of 0.20.

IV. Demonstration Calculations

A FORTRAN computer program was written with an algorithm based on the procedures outlined in Secs. II. and III. A set of demonstration calculations were performed assuming salt water droplets (solvent => water, solute => NaCl) with CO_2 laser heating [λ_{abs} = 10.6 μm, $\bar{n}_{abs}$ = (1.179, 0.072)] and He-Ne laser elastic scattering [λ_{sca} = 0.633 μm, $\bar{n}_{sca}$ = (1.332, 1.47 e-08)]. Pure water properties were used for $c_d(T)$, $h_{fg}(T)$, $k(T)$, $D(T,p)$, and $p_g(T)$. The droplet mass density, $\rho_d[T,(m_s/m_w)]$, was evaluated including both the effects of temperature and salt concentration. Curvefits for the absorption efficiency, Q_{abs}, and the nondimensionalized far-field scattering intensity, $\tilde{S}_r$, as a function of particle size parameter, $\alpha = 2\,\pi\,r_d / \lambda$, were generated using a previously developed computer program (Lorenz-Mie, plane wave on a sphere electromagnetic interaction). A graphical presentation of $Q_{abs}(\alpha_{abs})$ and $\tilde{S}_r(\alpha_{sca})$ are given, respectively, in Figs. 2 and 3.

The nominal conditions for the calculations that follow are T_∞ (ambient temperature) = 20 °C, p_∞ (ambient pressure) = 101.3 kPa, and T_{do} (initial droplet temperature) = 20 °C. A log-normal droplet distribution is assumed with a log-normal standard deviation parameter of σ_{DL} = 0.20 and a log-normal mean diameter, $\bar{D}_L$, of either 0.50, 1.00, 2.00, or 4.00 microns. The infrared (heating) laser beam is chopped (i.e., square wave with an intensity varying from zero to I_o) with a nominal intensity of I_o = 1.0 MW/m^2. The total elastic far-field scattering intensity expression, $\tilde{S}_r)_{tot}$, was computed (nominally) for a geometrical arrangement corresponding to pure backscattering ($\theta_{dir} = 180°$, $\phi_{dir} = 90°$).

A. Time Constants

Characteristic time constants for laser-on (τ_{on}) and for laser-off (τ_{off}) were determined by using a low frequency modulation (2.5 Hz or 5.0 Hz) so that the aerosol size distribution would reach equilibrium before the laser is switched back off/on. The time constant was defined as the time it took the far-field scattering to recover 63.2 % (i.e., 1 - e^{-1}) of the overall difference of the laser-on versus laser-off far-field scattering. Figure 4 shows the low frequency time variation of the far-field total scattering for the four different log-normal mean diameter size distributions. A plot of the corresponding calculated time constants, both for laser-on and for laser-off, versus mean diameter, is given in Fig. 5. As seen in Figs. 4 and 5, the laser-on (i.e., heating) time constant increases almost linearly with increasing aerosol mean diameter. For the small diameters (0.5 micron and 1.0 micron), the laser-off and laser-on time constants are approximately equal. However, for mean diameters greater than 1.0 micron, the laser-off time constant is significantly longer than the laser-on time constant and the laser-off time constant may either increase or decrease with increasing mean diameter (see Fig. 5).

The time constant results in Figs. 4 and 5 were for a nominal infrared (heating) laser intensity of 1.0 MW/m^2. The effect of laser intensity on the time constants was investigated and the results are shown in Figs. 6 and 7. For the 1.0 micron diameter distribution (Fig. 6), the time constants decreased slightly with increasing laser intensity. For the 2.0 micron distribution (Fig. 7) the laser-on time constant decreased significantly with increasing laser intensity while the laser-off time constant increased slightly with increasing laser intensity.

The time constant results in Figs. 4 and 5 were for a nominal ambient relative humidity of 90%. The effect of ambient relative humidity on the time constants was investigated and the results are shown in Figs. 8 and 9. For the 1.0 micron diameter distribution (Fig. 8), the time constants (both laser-on and laser-off) increased significantly with increasing ambient relative humidity. For the 2.0 micron distribution (Fig. 9), the laser-on time constant increased slightly and the laser-off time constant increased significantly with increasing ambient relative humidity.

B. Frequency Response

Systematic calculations were also performed investigating the effects of laser heating modulation frequency on the subsequent total far-field scattering. Figure 10 shows the 0.5 micron mean diameter total far-field scattering intensity as a function of time for the nominal conditions and modulation frequencies of 5, 10, 20, 50, 100, and 200 Hz. As seen in Fig. 10., for the 0.5 micron mean diameter, the peak-to-peak far-field scattering intensity is approximately constant for frequencies up to 50 Hz, and then decreases slightly as the frequency is increased to 100 Hz and then decreases significantly as the frequency is increased to 200 Hz. Similar time-varying far-field scattering intensity plots are provided for mean diameters of 1.0 microns, 2.0 micron, and 4.0 micron, respectively, in Figs. 11, 12, and 13. The "cut-off" frequency at which the total far-field scattering begins to decrease apparently decreases with increasing mean diameter. This observation is quantified in Fig. 14, where the normalized standard deviation of the total far-field scattering intensity (normalized relative to the mean value of the total far-field scattering intensity) is plotted versus frequency. As can also be seen in Figs. 12 and 14, the relative variation of total far-field scattering is particularly large for the 2.0 micron mean diameter distribution.

V. Possible Future Work

A theoretical modeling of the photothermal modulation of Mie scattering spectroscopy technique has been developed and demonstration calculations have been performed. Appropriate simplifying assumptions were applied in developing this initial modeling. Possible future work includes the following.

1.) Direct comparisons between experimental measurements and corresponding model calculations are needed to verify the overall correctness of the model and to verify the validity of the simplifying assumptions.

2.) The form of Raoult's law used in Sec. II is valid for low solute concentrations. A thorough literature search could be performed to see if a more rigorous, and more wide-ranging, form of Raoult's law can be identified. In addition, the effect of surface tension on Raoult's law was omitted (probably a good assumption except for very small droplets) and this effect could be included in a more advanced form of Raoult's law.

3.) The effects of solute concentration on droplet properties, in particular the complex index of refraction at both the laser heating and laser scattering wavelengths, needs further study.

4.) A finite-difference analysis could be performed to investigate the correctness of the quasi-steady boundary layer assumption for the modeling of the mass transfer and heat transfer at the droplet surface. If necessary, corrections could be incorporated into the model.

5.) A uniform droplet temperature was assumed. This is probably a good assumption for relatively small droplets and low modulation frequencies. However, the possible effects of distributed heating could be investigated.

VI. References

ARMSTRONG, R.L., "Aerosol heating and vaporization by pulsed light beams," Applied Optics, Vol. 23, pp. 148-155, 1984.

ARMSTRONG, R.L., S.A.W. Gerstl, and A. Zardecki, "Nonlinear pulse propagation in the presence of evaporating aerosols," Journal of the Optical Society of America A, Vol. 2, pp. 1739-1746, 1985.

ARNOLD, S., E.K. Murphy, and G. Sageev, "Aerosol particle molecular spectroscopy," Applied Optics, Vol. 24, pp. 1048-1053, 1985.

BARTON, J.P., D. R. Alexander, S. A. Schaub, "Internal and near-surface electromagnetic fields for a spherical particle irradiated by a focused laser beam," Journal of Applied Physics, Vol. 64, pp. 1632-9, 1988.

BARTON, J.P., D. R. Alexander, and S. A. Schaub, "Internal fields of a spherical particle illuminated by a tightly focused laser beam: focal point positioning effects at resonance," Journal of Applied Physics, Vol. 65, pp. 2900-6, 1989.

BARTON, J.P. and D. R. Alexander, "Fifth-order corrected electromagnetic field components for a fundamental Gaussian beam," Journal of Applied Physics, Vol. 66, pp. 2800-2802, 1989.

BARTON, J.P., "Light scattering calculations for irregularly-shaped axisymmetric particles of homogeneous and layered composition," Measurement Science and Technology, Vol. 9, pp. 151-160, 1998.

CAMPILLO, A.J., C.J. Dodge, and H.-B. Lin, "Aerosol particle absorption spectroscopy by photothermal modulation of Mie scattered light," Applied Optics, Vol. 20, pp. 3100-3103, 1981.

CHAN, C.H. "Effective absorption for thermal blooming due to aerosols," Applied Physics Letters, Vol. 26, pp. 628-630, 1975.

CHEEKATI, P.B. "Monte Carlo analysis of laser pulse propagation within an aerosol spray," Masters Thesis (J.P. Barton, adviser), Mechanical Engineering Department, University of Nebraska-Lincoln, 1993.

DAVIES, S.C. and J.R. Brock, "Laser evaporation of droplets," Applied Optics, Vol. 26, pp. 786-793, 1987.

FERRON, G.A. and S.C. Soderholm, "Estimation of the times for evaporation of the pure water droplets and for stabilization of salt solution particles," Journal of Aerosol Science, Vol. 21, pp. 415-429, 1990.

GATHMAN, S.G., "Optical properties of the marine aerosol as predicted by the Navy aerosol model," Optical Engineering, Vol. 22, pp. 57-62, 1983.

GOOTY, P.A., "Numerical analysis of transient heat transfer in laser-heated cylindrical particles," Masters Thesis (J.P. Barton, adviser), Mechanical Engineering Department, University of Nebraska-Lincoln, 1992.

GRACHEV, Y.N. and G.M. Strelkov, "Convective evaporation of a water drop in a radiation field," Soviet Journal of Quantum Electronics, Vol. 4, pp. 1221-1223, 1975.

INCROPERA, F.P. and D.P. DeWitt, *Fundamentals of Heat and Mass Transfer*, 3rd ed., John Wiley & Sons, New York, 1990.

KAYS, W.M., *Convective Heat and Mass Transfer*, McGraw Hill, New York, 1966.

KNEER, R., M. Schneider, B. Noll, and S. Wittig, "Diffusion controlled evaporation of a multicomponent droplet: theoretical studies on the importance of variable liquid properties," International Journal of Heat and Mass Transfer, Vol. 36, pp. 2403-2415, 1993.

LATIFI, H., J.-G. Xie, T.E. Ruekgauer, R.L. Armstrong, and R.G. Pinnick, "Multiple superheating thresholds of micrometer-sized droplets irradiated by pulsed CO_2 lasers," Optics Letters, Vol. 16, pp. 1129-1131, 1991.

LIN, H.-B. and A.J. Campillo, "Photothermal aerosol absorption spectroscopy," Applied Optics, Vol. 24, pp. 422-433, 1985.

LU, Q.J. and N. Fukuta, "Heating of hygroscopic aerosol in moist air," Journal of Aerosol Science, Vol. 21, pp. 777-783, 1990.

LU, W. and W.M. Worek, "Two-wavelength interferometric technique for measuring the refractive index of salt-water solutions," Applied Optics, Vol. 32, pp. 3992-4002, 1993.

MARGERIT, J. and O. Sero-Guillaume, "Study of the evaporation of a droplet in its stagnant vapor by asymptotic matching," International Journal of Heat and Mass Transfer, Vol. 39, pp. 3887-3898, 1996.

PARK, B.-S. and R.L. Armstrong, "Laser droplet heating: Fast and slow heating regimes," Applied Optics, Vol. 28, pp. 3671-3680, 1989.

PRISHIVALKO, A.P. and S.T. Leiko, "Radiative heating and evaporation of droplets," Soviet Journal of Applied Spectroscopy, Vol. 33, pp. 1137-1142, 1980.

RENKSIZBULUT, M. and M. Bussmann, "Multicomponent droplet evaporation at intermediate Reynolds numbers," International Journal of Heat and Mass Transfer, Vol. 36, pp. 2827-2835, 1993.

SAGEEV, G. and J.H. Seinfeld, "Laser heating of an aqueous aerosol particle," Applied Optics, Vol. 23, pp. 4368-4374, 1984.

SASSEN, K. "Infrared (10.6 micron) radiation induced evaporation of large water drops," Journal of the Optical Society of America, Vol. 71, pp. 887-891, 1981.

SCHENKEL, A. and K. Schaber, "Growth of salt and acid aerosol particles in humid air," Journal of Aerosol Science, Vol. 26, pp. 1029-1039, 1995.

TANG, I.N. "Phase transformation and growth of aerosol particles composed of mixed salts," Journal of Aerosol Science, Vol. 7, pp. 361-371, 1976.

TANG, I.N. and H.R. Munkelwitz, "Aerosol growth studies -- III Ammonium bisulfate aerosols in a moist atmosphere," Journal of Aerosol Science, Vol. 8, pp. 321-330, 1977.

YALAMOV, Y.I., E.R. Shchukin, V.B. Kutukov, and V.L. Malyshev, "Diffusional evaporation of drops in a field of electromagnetic radiation with arbitrary temperature drops," Soviet High Temperature, Vol. 15, pp. 370-373, 1977.

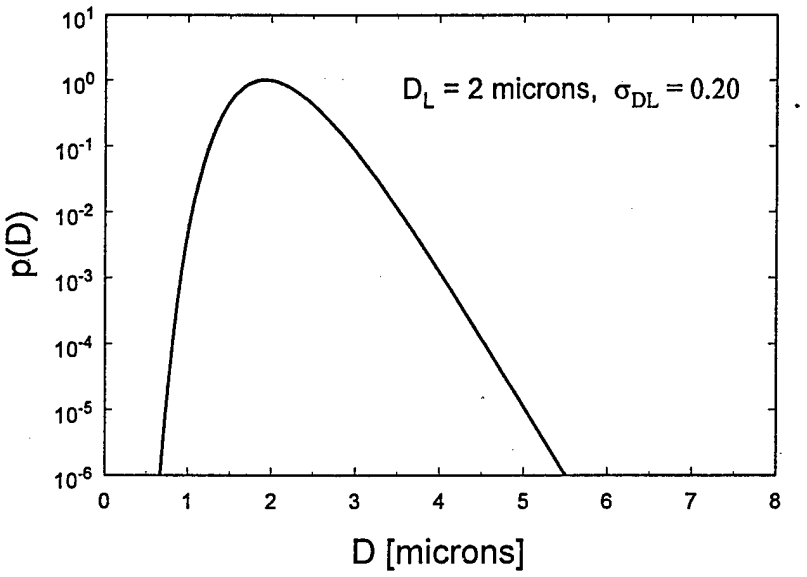

Fig. 1. Log-normal probability density distribution function with a log-normal mean diameter ($\bar{D}_L$) of 2.0 microns and a log-normal standard deviation parameter (σ_{DL}) of 0.20.

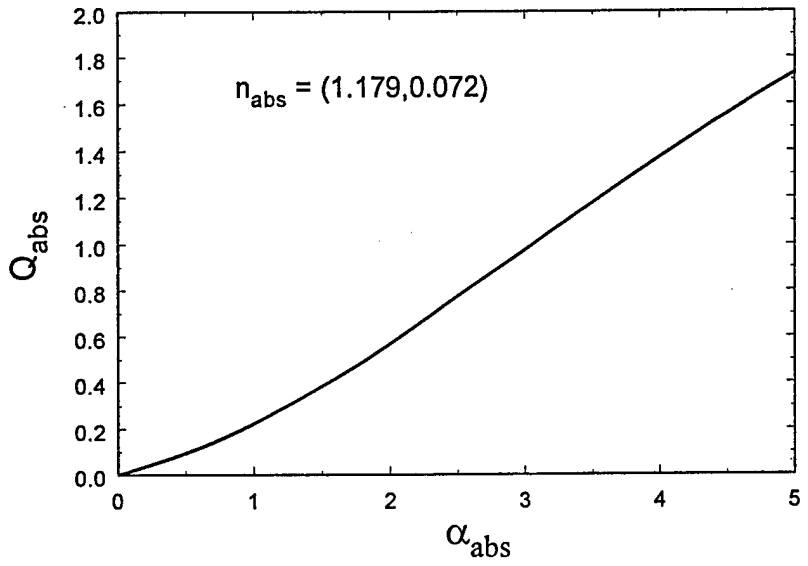

Fig. 2. Absorption efficiency as a function of size parameter, λ_{abs} = 10.6 μm, $\bar{n}_{abs}$ = (1.179,0.072).

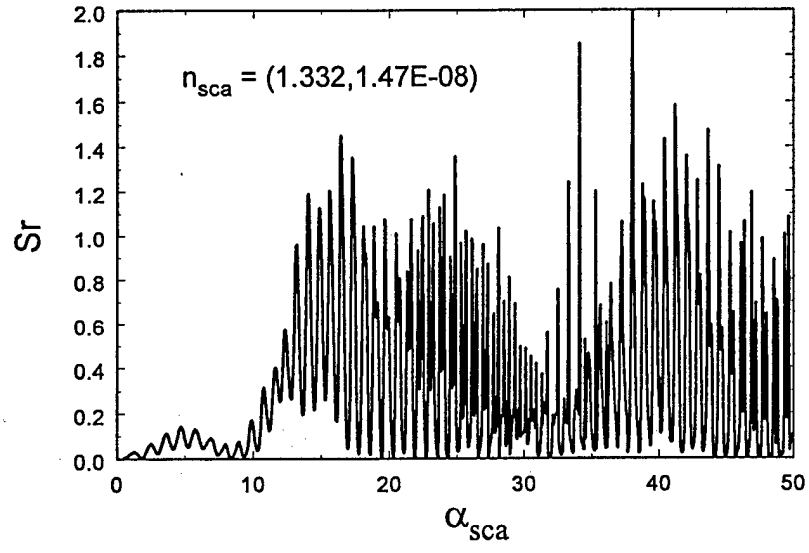

Fig. 3. Nondimensionalized far-field scattering intensity ($\tilde{S}_r$) for pure backscatter (θ_{dir} = 180°,ϕ_{dir} = 90°) as a function of size parameter, λ_{sca} = 0.633 μm, $\bar{n}_{sca}$ = (1.332,1.47E-08).

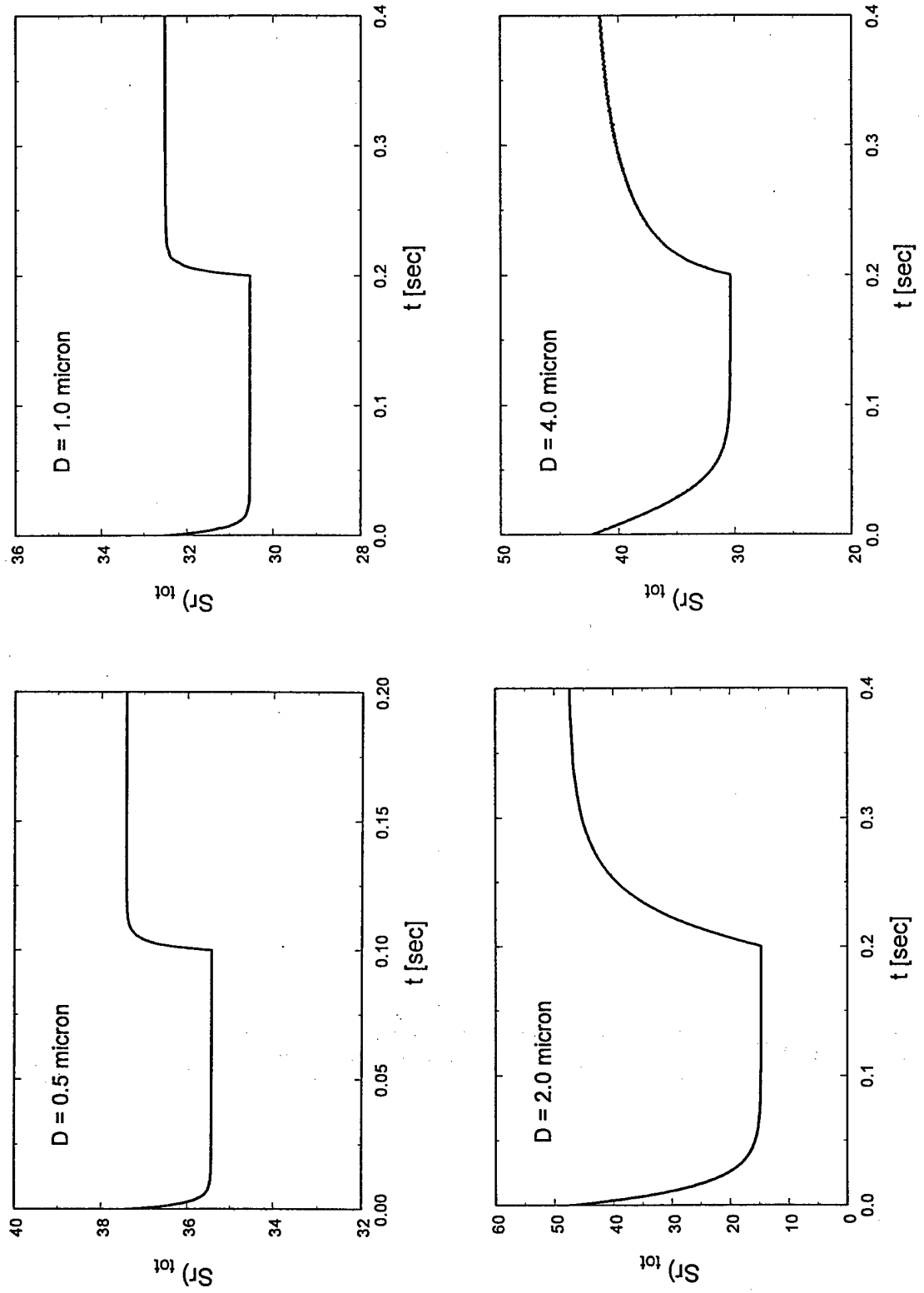

Fig. 4. Total far-field scattering at low frequency modulation.

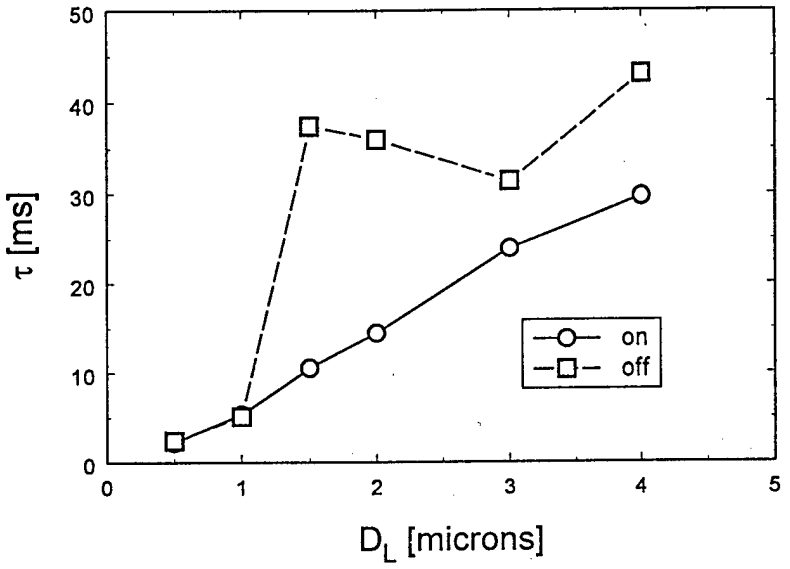

Fig. 5. Laser-on and laser-off far-field scattering time constants as a function of aerosol mean diameter.

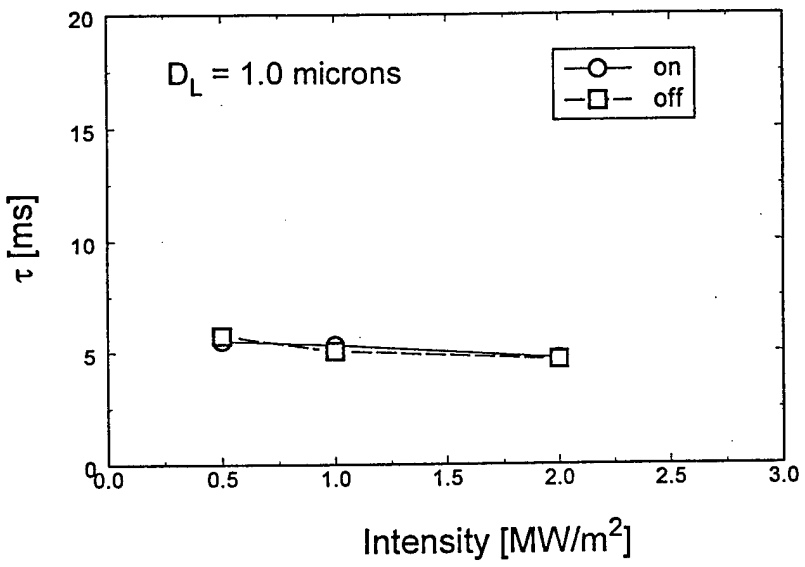

Fig. 6. Laser-on and laser-off far-field scattering time constants as a function of heating laser intensity. Log-normal mean diameter equal to 1.0 micron.

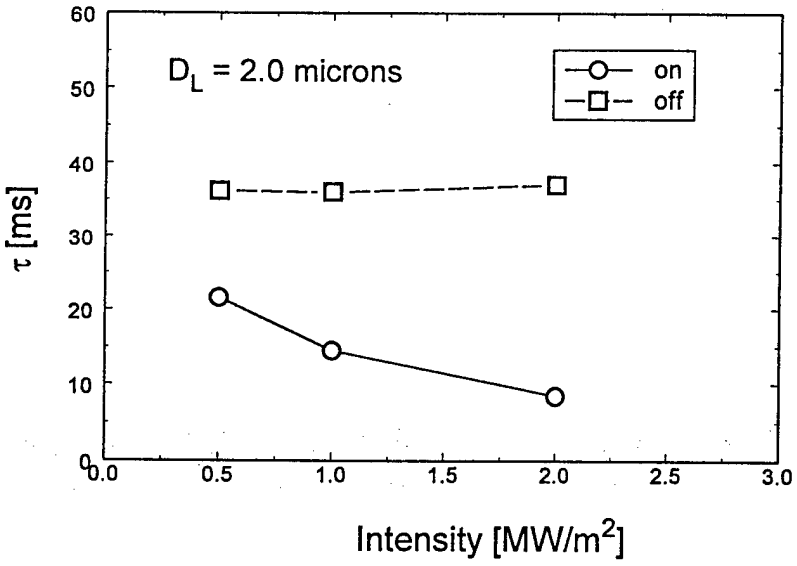

Fig. 7. Laser-on and laser-off far-field scattering time constants as a function of heating laser intensity. Log-normal mean diameter equal to 2.0 micron.

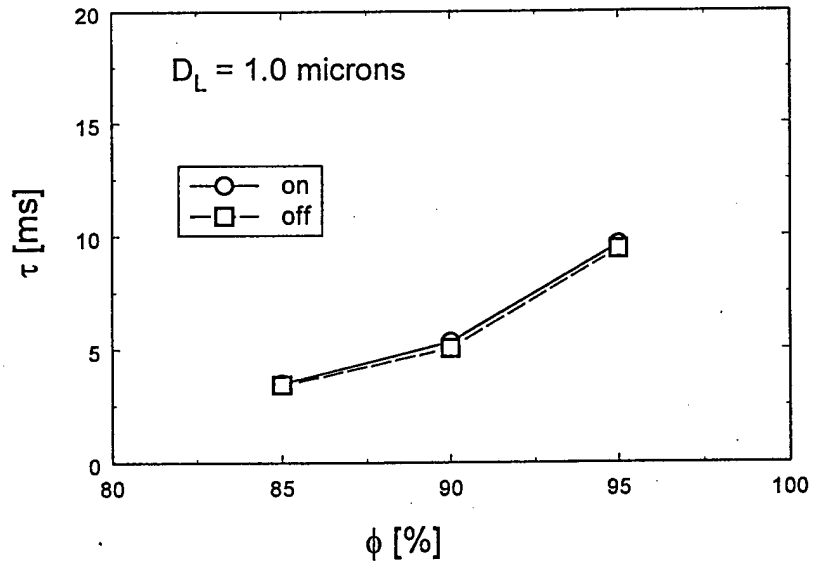

Fig. 8. Laser-on and laser-off far-field scattering time constants as a function of ambient relative humidity. Log-normal mean diameter equal to 1.0 micron.

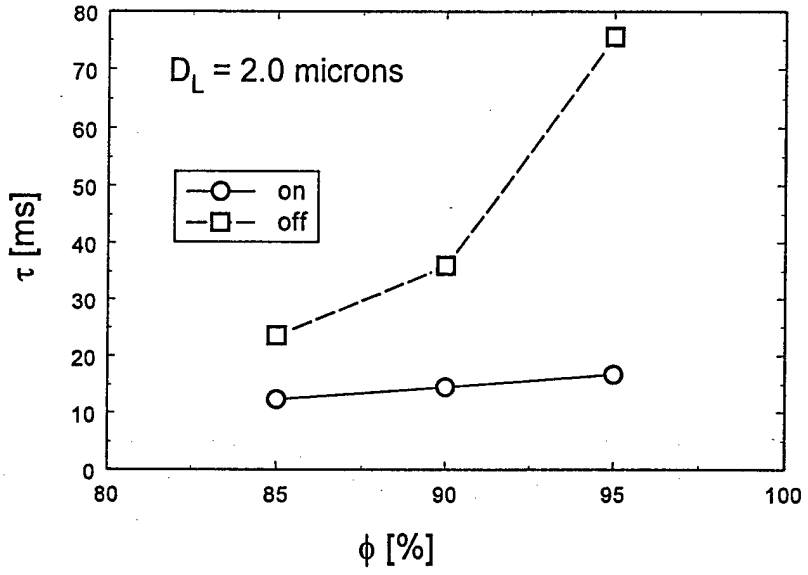

Fig. 9. Laser-on and laser-off far-field scattering time constants as a function of ambient relative humidity. Log-normal mean diameter equal to 2.0 micron.

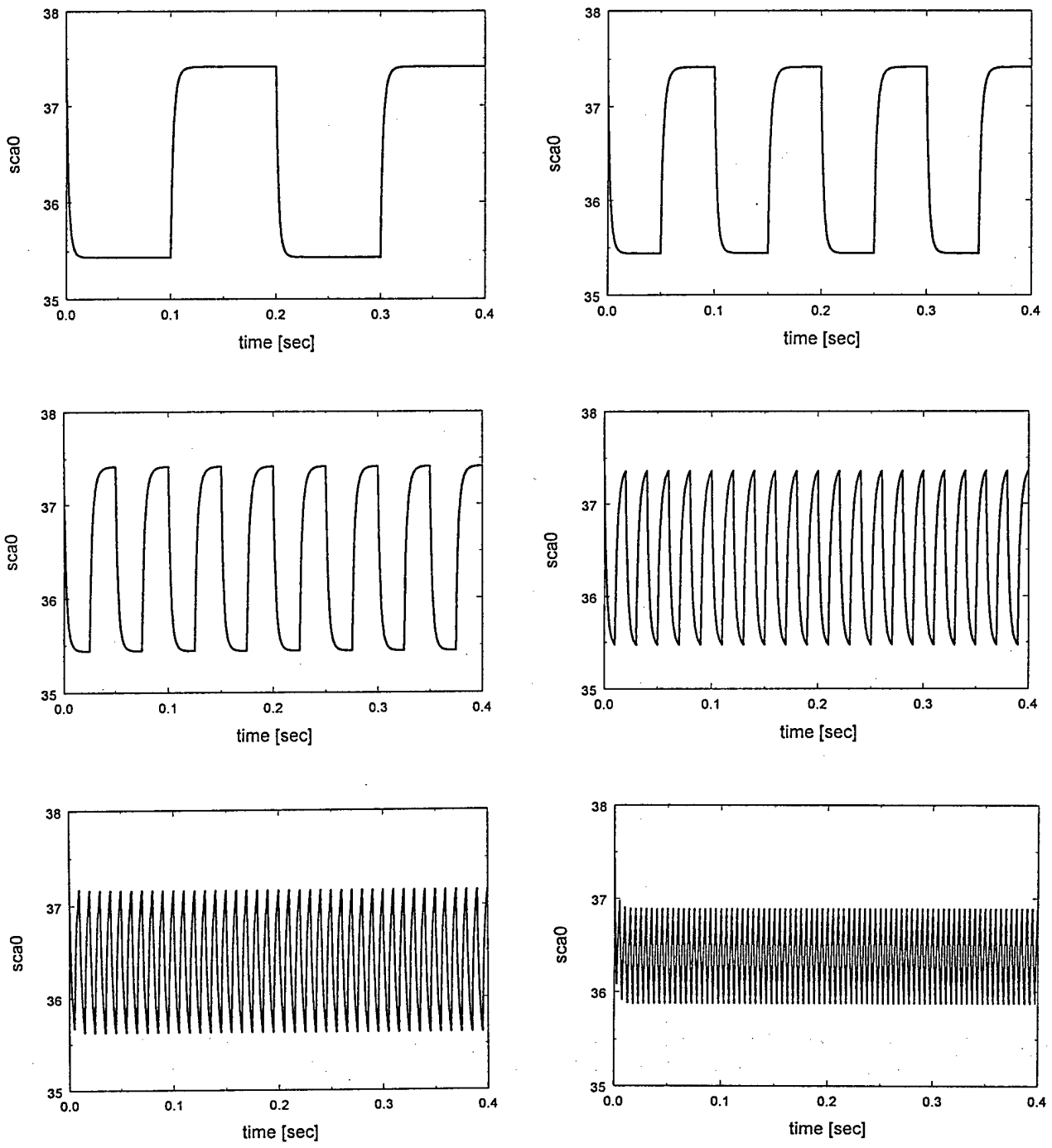

Fig. 10. Total far-field scattering versus time for modulated heating laser intensity at modulation frequencies of 5, 10, 20, 50, 100, and 200 Hz. Log-normal mean diameter equal to 0.5 micron.

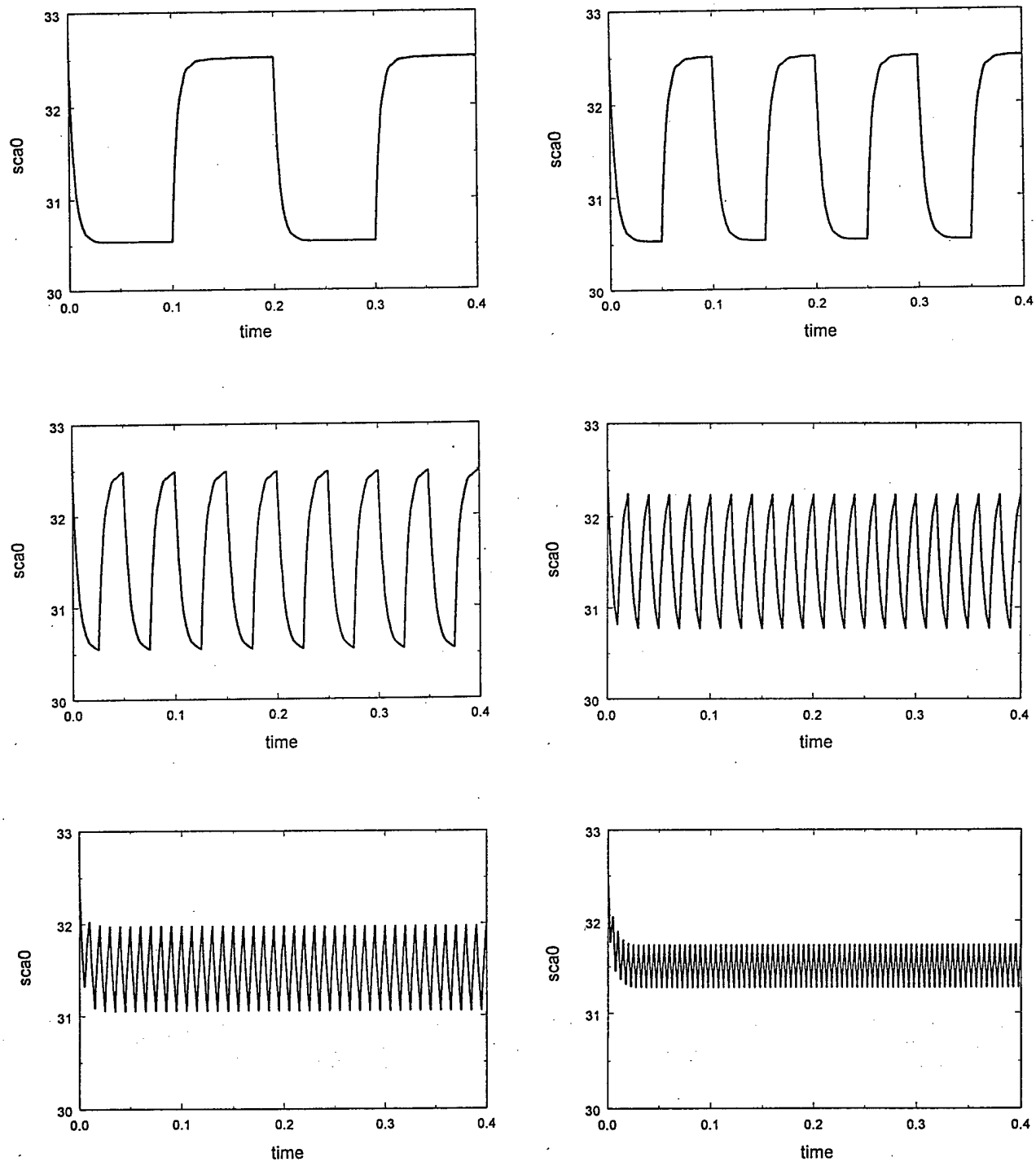

Fig. 11. Total far-field scattering versus time for modulated heating laser intensity at modulation frequencies of 5, 10, 20, 50, 100, and 200 Hz. Log-normal mean diameter equal to 1.0 micron.

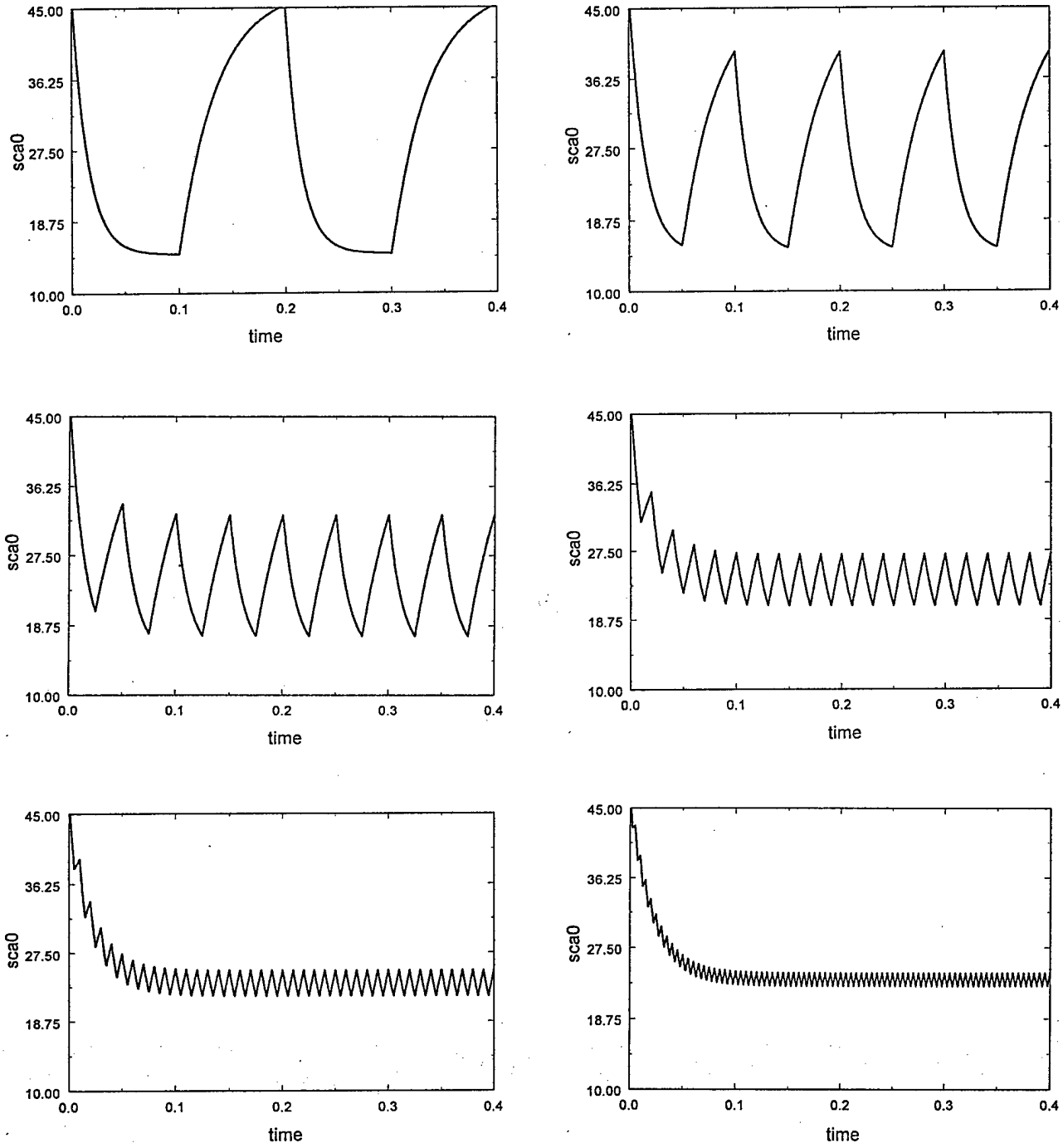

Fig. 12. Total far-field scattering versus time for modulated heating laser intensity at modulation frequencies of 5, 10, 20, 50, 100, and 200 Hz. Log-normal mean diameter equal to 2.0 micron.

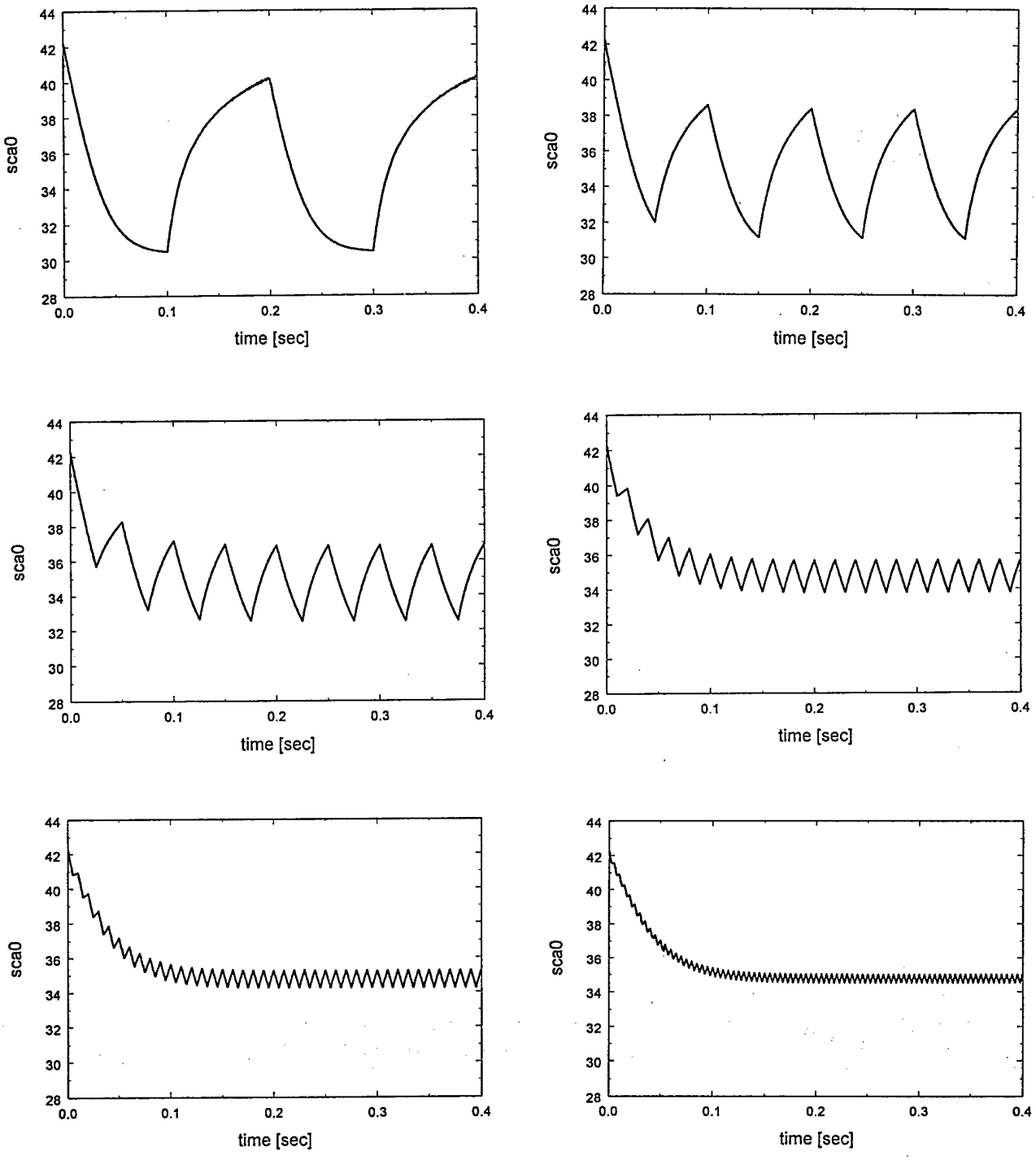

Fig. 13. Total far-field scattering versus time for modulated heating laser intensity at modulation frequencies of 5, 10, 20, 50, 100, and 200 Hz. Log-normal mean diameter equal to 4.0 micron.

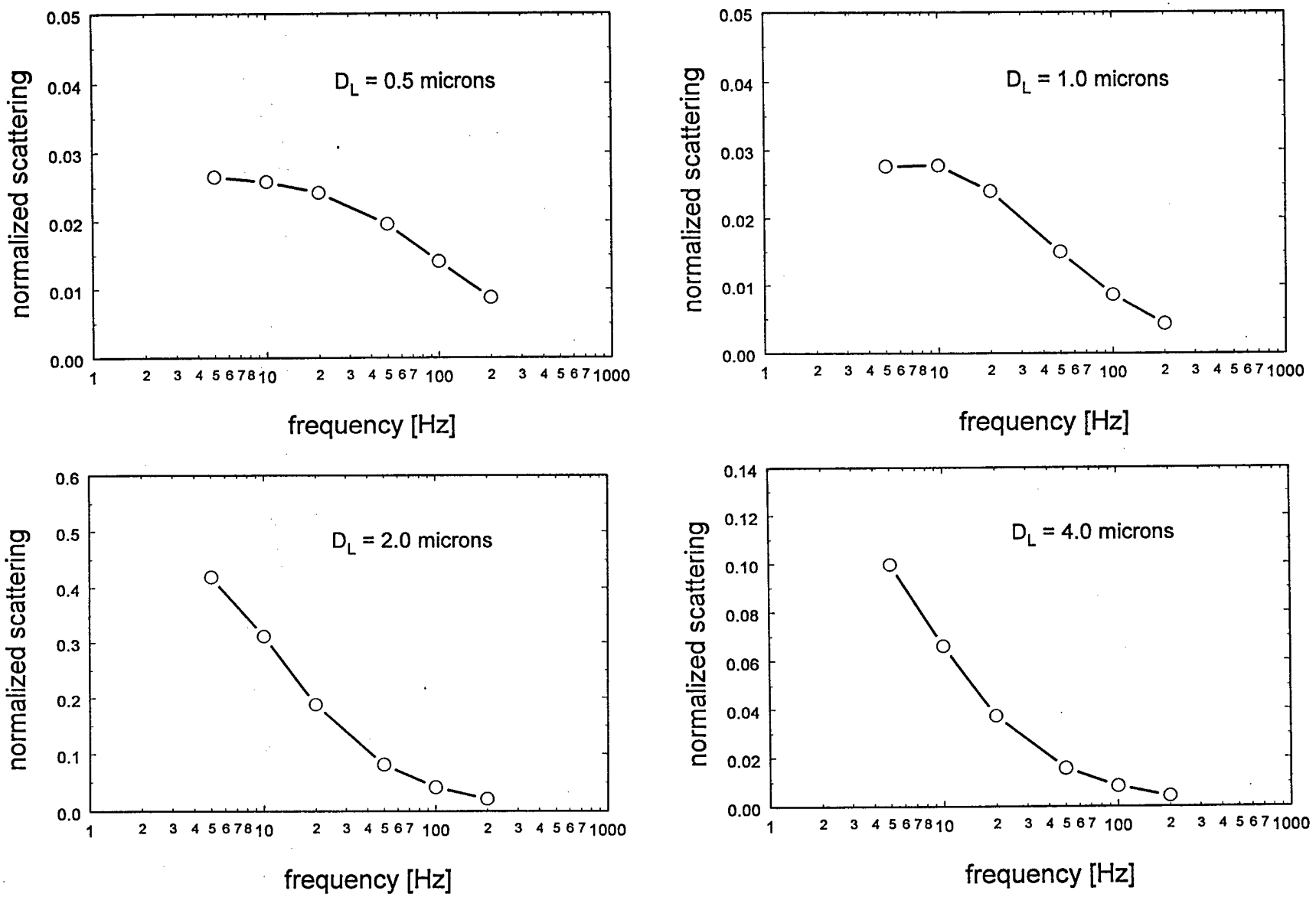

Fig. 14. Normalized standard deviation of total far-field scattering intensity as a function of modulation frequency for log-normal mean diameters of 0.5, 1.0, 2.0, and 4.0 microns.